RESEARCH ARTICLE

ER exit sites (ERES) and ER–mitochondria encounter structures (ERMES) often localize proximally

Naini Chakraborty[1,2] (iD), Bhawik Kumar Jain[1,2], Samruddhi Shembekar[1] and Dibyendu Bhattacharyya[1,2,3] (iD)

1 Department of Cell and Tumor Biology, Advanced Centre for Treatment Research & Education in Cancer (ACTREC) Tata Memorial Centre, Navi Mumbai, India
2 Homi Bhabha National Institute, Mumbai, India
3 Department of Internal Medicine, University of Michigan, Ann Arbor, MI, USA

To understand the potential interplay between vesicular trafficking and direct membrane contact sites-mediated transport, we selected the endoplasmic reticulum (ER), which participates in both modes of inter-organelle transport. ER–mitochondria encounter structures (ERMES) are direct membrane contact junctions that mediate macromolecule exchange, while the secretory pathway originates at ER exit sites (ERES). Using the budding yeast *Pichia pastoris*, we documented that ERMES resident proteins are often juxtaposed with ERES markers. We further demonstrated that ERES form *de novo* almost always near a pre-existing ERMES. Disruption of either ERES or ERMES affects the other. Djp1, a chaperone reported to mediate mitochondrial import of ER-resident proteins, localizes at the ERES–ERMES proximal region. Our results indicate a potential functional link between ERES–ERMES proximity and mitochondrial protein import.

Keywords: ER; ERES; ERMES; Golgi; mitochondria

Inter-organelle communication becomes challenging and critical in crowded intracellular environments. Organelles communicate with each other chiefly *via* two ways – vesicular trafficking and direct membrane contact-based transport [1,2]. The endoplasmic reticulum (ER), the central hub for protein and lipid biosynthesis, is involved in both modes of inter-organelle communication.

Vesicular transport includes mainly the ER, Golgi and various other organelles, along with a series of cargo-carrying secretory vesicles forming at ER exit sites (ERES). These vesicles fuse and gradually mature towards developing the Golgi network, where numerous functions, including modification of secretory cargoes and sorting, occur, followed by delivery to their target destinations [3].

The direct membrane contact-based transport is mediated by the tethering between two organelles. These direct connections, termed membrane contact sites (MCSs), represent zones of proximity (10–30 nm) between two organelles [4]. Inter-organelle contacts are found for multiple organelles and likely mediate the direct exchange of metabolites and information between organelles. Specifically, ER and mitochondria exchange various biomolecules for different cellular functions. Aberrant inter-organelle contacts between the ER and mitochondria are associated with human neurodegenerative diseases [5]. Tethering between ER and mitochondria was initially observed in rat liver cells [6–9]. However, the structure and functions of such putative contacts between ER and mitochondria and their components are being recently

---

Abbreviations

ER, endoplasmic reticulum; ERES, ER exit sites; ERMES, ER–mitochondria encounter structures; MCS, membrane contact sites.

investigated and unravelled in mammalian systems [10,11]. The molecular tether termed 'ERMES' (ER–mitochondria encounter structure) between the two organelles, ER and mitochondria, was reported in *Saccharomyces cerevisiae* as distinct puncta [2,12,13]. The ERMES is composed of four components, namely Mmm1 (ER component), Mdm12 (cytosolic factor), Mdm10 and Mdm34 (outer mitochondrial membrane component). Mmm1 is a transmembrane protein embedded in ER, while Mdm34 and Mdm10 are present in the outer mitochondrial membrane (OMM). Mdm10 is a beta-barrel protein that also participates in forming a part of the SAM complex (protein sorting and assembly machinery) in OMM [14–17]. The tethering complex localized to discrete foci suggested the presence of distinct sites of close apposition between ER and mitochondria. Previous reports suggest that loss of ERMES (deletion of ERMES components) results in severe growth defects and altered mitochondrial morphology in *S. cerevisiae*. [13]. The ERMES junction facilitates inter-organelle calcium transport and phospholipid exchange and maintains mitochondrial morphology [2,18,19]. Previous studies illustrated that ERMES mutants are known to manifest defective mitochondrial morphology, mtDNA maintenance, mitochondrial protein import and growth, especially in non-fermentable media [20]. Initially, the ERMES study has been primarily confined to the fungi group. However, in recent years, analysis of such structures in higher eukaryotes has also been reported [10,21].

The two modes of transport are thus physiologically important in all living cells. However, very little is known about any functional crosstalk between these two different modes of intracellular organelle communications. Although molecule exchange *via* vesicular trafficking has been extensively studied, communication *via* direct connections or junctions between organelles is a relatively new concept. A recent study highlighted an early component of the secretory pathway, Sar1, responsible for the biogenesis of ERES [22], to be also involved in regulating the curvature at the ER–mitochondria interface and hence the ER–mitochondria contacts in *S. cerevisiae* [23]. We wanted to understand the interplay of the two modes of inter-organelle communication pathways and we chose the budding yeast *Pichia pastoris* as our model system for the study. *Pichia pastoris* has a highly evolved secretory pathway. It has well-defined, discrete ER exit sites and stacked Golgi cisterna as compared to *S. cerevisiae* which has several ERES and unstacked Golgi

cisterna [24–26]. However, ERMES has not yet been characterized in *P. pastoris*.

We thus undertook investigations to check the existence of ERMES in *P. pastoris* by detecting its individual components and demonstrating their co-localization by fluorescent imaging. Ours is the first report to show that ERMES do exist in *P. pastoris* and that ERES and ERMES are juxtaposed and show partial overlap. Furthermore, to understand whether there is any structural/functional correlation between the above-mentioned sites, we used the anchor-away approach. Anchor-away assay is a ligand-based method that is used to mislocalize a component of a target site to another cellular location in a spatio-temporal manner, where it is rendered non-functional. The effect of such mislocalization of components of one site on the other site was determined in these assays. Disruption of either ERES or ERMES leads to alterations in the copy number of the other, and de-coupling of ERMES-ERES proximity.

Mitochondrial protein import is relatively poorly understood for proteins synthesized by cytosolic ribosomes. The ER surface has been implicated as a trap as well as transit space for their mitochondrial targeting. Earlier reports have highlighted the existence of a wide array of machinery and mechanism which co-operate with the aid of molecular chaperones and assembly complexes to direct the import and sorting of mitochondrial precursor proteins that are synthesized on cytoplasmic ribosomes to their correct destination effectively. [27,28]. A recent study in yeast (*S. cerevisiae*) suggested the existence of this 'ER-SURF' pathway which retrieves mitochondrial proteins from the ER surfaces, re-routing them to mitochondria with the help of an ER-localized chaperone Djp1 [29]. But, the initial stages of this ER-based mito-protein targeting are unclear. In the present study, we observed that Djp1, an ER-localized chaperone, localizes in the spatial proximity of ERES–ERMES overlap, in closer proximity with ERES than ERMES. Our observations suggest that such a close association between these two functional sites (ERES and ERMES) may influence the 'ER-SURF' pathway *via* which mitochondrial import of proteins occurs with the aid of Djp1. Altogether, our results indicate a novel chaperone-based retrieval of mitochondrial bound cargo mediated in the vicinity of the spatial overlap of ERES–ERMES.

Altogether, ours is the first report which documents a plausible co-operative relationship between vesicular (ERES) and non-vesicular transport mechanisms (ERMES).

Materials and methods

General yeast manipulation and molecular biology methods

All experiments with *P. pastoris* were performed using the haploid wild-type strain PPY12 (his4 arg4) [30], and its derivatives are listed in Table S2. General methods for the growth and transformation of *P. pastoris* used in this study were as described previously [31]. All the cultures were grown in rich glucose medium (YPD), synthetic glucose medium (SD) or non-fluorescent synthetic glucose medium (NSD) [26] in baffled flasks at 30 °C with shaking conditions at 1 *g*. The strains were selected on YPD media supplemented with G418 (500 µg·mL^{-1}) or hygromycin B (250 µg·mL^{-1}) or SD medium depending on respective integrating plasmids. Transformation of *P. pastoris* was performed with linearized integrating vectors carrying tagged gene of interest using the electroporation method. *P. pastoris* gene sequences were obtained from the NCBI database. Molecular biology procedures were simulated and recorded using SNAPGENE software (Dotmatics, Boston, MA, USA). All plasmids used in this study are listed in Table S1.

To create functionally inactivated proteins by mislocalization from its function zone to another cellular location using the anchor-away method

The construction of a PPY12 derivative suitable for anchor-away experiments was described previously [32]. The same parent anchor-away strain was obtained from Glick lab and is used in this study to create all the ERMES anchor-away strains. Briefly, in the PPY12 derivative anchor-away strain, the TOR1 gene was modified to confer rapamycin resistance, the FPR1 gene was deleted and the ribosomal protein Rpl17 was C terminally tagged with FKBPx4. The protein to be inactivated was tagged with 2XFRB or 2XFRBGFP by gene replacement. Yeast cells grown to mid-log phase [0.5 optical density at 600 nm (OD600)] were treated with 1 µg·mL^{-1} rapamycin added from a stock of 2 mM made in 90% ethanol/10% Tween 20, and were imaged after ∼ 10 min along with the control that is the untreated sample.

Growth curve assay

To check whether the fluorescent tags fusion proteins affect the growth of the wild-type yeast cells, a growth-based biochemical assay using the *P. pastoris* system was developed. We designed a fluorescent fusion construct by integrating the coding sequence of GFP/mCherry into the C terminus of the nuclear-encoded proteins (target markers used in the study) and cloning it into their respective vector (cloning strategies for individual fluorescent marker proteins are explained in detail in the subsequent sections). We then transformed the linearized DNA into the *P. pastoris* strain (WT-PPY12). We individually grew all the PPY12 derivative yeast strains containing the fluorescently labelled target markers along with wild-type strain in a rich glucose medium (YPD media). We checked its growth by measuring absorbance at 600 nm (OD-600) for 8 h (0–8 h) and plotted the growth curve (Fig. S8B).

Construction of yeast strains expressing tagged Mmm1

The full-length *P. pastoris* MMM1 plus a downstream region were amplified by PCR. This fragment was digested with EcoRI and SphI and ligated into the pUC19-ARG4 vector digested with the same sets of enzymes. BamHI and NotI sites were introduced by site-directed mutagenesis in place of the stop codon. An mEGFP cassette from the pmEGFPC1 vector was excised with BamHI and NotI and inserted. The resultant plasmid was linearized with PstI and integrated at the *PpMMM1* locus. For swapping of epitope tags, a 3XmCherry fragment was digested with BamH1 and Not1 and ligated to create Mmm1-3xmCherry. The resultant plasmids were linearized with PstI and integrated at the *PpMmm1* locus. To swap the drug resistance marker, Mmm1EGFP was PCR amplified and digested with SacI and SpeI and ligated in pAG32 vector [33] digested with the same enzymes. The resultant plasmids were linearized with MscI and integrated at the *PpMMM1* locus, followed by selection with hygromycin B. For creating anchor-away strains, cassettes encoding FRBGFP and FRB were excised with BamHI and NotI from constructs called pblue.2x (4GSS-FRB). HA.GFP and pblue.2x (4GSS-FRB).HA [32] were inserted in the BamH1-Not1-mutagenized pUC19ARG-Mmm1 construct. These plasmids were linearized with PstI and integrated at the *PpMMM1* locus.

Construction of yeast strains expressing tagged Mdm10

The full-length *P. pastoris* MDM10 plus a downstream region were amplified by PCR. This fragment was digested with EcoRI and SphI and ligated into the pUC19-ARG4 vector digested with the same sets of enzymes. BamHI and NotI sites were introduced by site-directed mutagenesis in place of the stop codon. An mEGFP cassette from the pmEGFPC1 vector was excised with BamHI and NotI and inserted. The resultant plasmid was linearized with HpaI and integrated at the *PpMDM10* locus. For swapping of epitope tags, a 3XmCherry fragment was digested with BamHI and Noti and ligated to create Mdm10-3xmCherry. The resultant plasmids were linearized with HpaI and integrated at the *PpMDM10* locus.

Construction of yeast strains expressing tagged Mdm34

The full-length *P. pastoris* MDM34 plus a downstream region were amplified by PCR. This fragment was digested with XmaI and HindIII and ligated into pUC19-ARG4 vector digested with the same sets of enzymes. BamHI and NotI sites were introduced by site-directed mutagenesis in place of the stop codon. An mEGFP cassette from the pmEGFPC1 vector was excised with BamHI and NotI and inserted. The resultant plasmid was linearized with XbaI and integrated at the *PpMDM34* locus. For swapping of epitope tags, a 3x-GFP 3x-mCherry and 6x-mCherry fragments were digested with BamH1 and Not1 and ligated to create Mdm34-3xGFP, Mdm34-3xmCherry and Mdm34-6xmCherry respectively. The resultant plasmids were linearized with XbaI and integrated at the *PpMDM34* locus. To swap the drug resistance marker, Mdm34 was PCR amplified and digested with SmaI and HindIII and ligated in pAG32 vector [33] digested with the same enzymes. A BamHI site was then introduced by site-directed mutagenesis. A cassette-encoding 3X-GFP and 6x-mCherry were excised with BamHI and HindIII and ligated to generate the resultant plasmid, which was linearized with XbaI and integrated at the *PpMDM34* locus, followed by selection with hygromycin B.

Construction of a yeast strain expressing tagged Tom70

The full-length *P. pastoris* TOM70 gene was amplified by PCR. This fragment was digested with BamHI and SmaI and subcloned into a pAG32 derivative expressing Mdm34-EGFP. From this vector (Mdm34-mEGFP-pAG32), the Mdm34 fragment was excised with BamHI and SmaI and replaced by an amplified Tom70 insert digested by the same restriction enzyme pair. The recombinant plasmid was linearized with MscI and integrated at the *PpTOM70* locus. This was followed by selection with hygromycin B.

Construction of yeast strains expressing tagged Sec63

The full-length *P. pastoris* SEC63 coding sequence plus a downstream region were amplified by PCR, and this fragment was inserted between the EcoRI and HindIII sites of pUC19-ARG4. BamHI and NotI sites were introduced by site-directed mutagenesis in place of the stop codon. A 3xmCherry cassette excised with BamHI and NotI was inserted. This plasmid was linearized with EcoNI and integrated at the *PpSEC63* locus. For swapping of drug resistance markers, the Sec63-3xmCherry fragment was digested with EcoRI and HindIII and ligated in the pIB1 vector [31] cut with the same enzyme. The resultant plasmid was linearized with AflII to integrate at the His4 locus.

Construction of a yeast strain expressing tagged HDEL

A construct, pIB2-DsRed-HDEL [26], was linearized with SalI and integrated at the HIS4 locus.

Construction of yeast strains expressing tagged Sec13

A plasmid for the expression of Sec13-EGFP [34] was modified by replacing EGFP with msGFP [35]. The Sec13-msGFP plasmid and a similar plasmid for expression of Sec13-DsRed [36] were linearized with MscI and integrated at the *PpSEC13* locus. For tag swapping, the segment encoding Sec13-DsRed was PCR amplified and then ligated to pUC19-ARG4 and pAG32 (hygro) vector. The resultant plasmids were linearized with MscI and integrated at the *PpSEC13* locus.

Construction of yeast strain expressing tagged Sec31

The plasmids expressing Sec31msGFP-pAG32 were linearized with EcoNI and integrated at the *PpSec31* locus followed by selection with hygromycin B.

Construction of yeast strains expressing tagged Sec23

For creating anchor-away strain, cassettes encoding FRBGFP were excised with BamHI and NotI from pblue.2x (4GSS-FRB). HA.GFP and ligated in pUC19-ARG4-PpSEC23-FRB-HA [32] construct digested with the same enzymes to replace tag FRB with FRBGFP. The resultant plasmid was linearized using KpnI and integrated.

Construction of yeast strains expressing tagged Djp1

The full-length *P. pastoris* Djp1 plus a downstream region were amplified by PCR. This fragment was digested with EcoRI and HindIII and ligated into pUC19-ARG4 vector digested with the same sets of enzymes. BamHI and NotI sites were introduced by site-directed mutagenesis in place of the stop codon. Cassettes encoding 3xGFP and 3xmCherry were excised with BamHI and NotI and inserted. The resultant plasmids were linearized with XbaI and integrated at the *PpDjp1* locus. To swap the drug resistance marker, Djp1 was PCR amplified and digested with SmaI and BamHI and ligated in pAG32-Mdm34-3xGFP vector digested with the same enzymes so that Mdm34 is replaced by Djp1. The resultant plasmids were linearized with XbaI and integrated at the *PpDjp1* locus, followed by selection with hygromycin B.

Fluorescence microscopy of yeast and quantification of fluorescence data

Live cell confocal imaging was performed with a Leica SP8 using a $100\times$ 1.4-NA objective. Cells were grown to log phase in YPD, immobilized on glass-bottom dishes using concanavalin A, washed, covered with SD or NSD and imaged at 30 °C [37]. Single- or dual-colour datasets were obtained using separate excitation and capture of red and green signals, with a pinhole of 1.2 A.U. and with a line averaging of 8. A pixel size of 60–70 nm, a frame size of 256×128 or 256×256 pixels and a Z-step interval of 0.30 μm were used. For 4D imaging, a previously described method was adapted [37,38]. Z-stacks were collected at intervals of 2 s. Deconvolution of image stacks was performed using HUYGENS PROFESSIONAL software (Scientific Volume Imaging, Hilversum, the Netherlands) and further processed using IMAGEJ [39]. Using IMAGEJ and ADOBE PHOTOSHOP, all the average projected fluorescence micrographs were assembled. Micrographs labelled 'merged' include transmitted light images of the cells. For static images, the overlap between two punctate fluorescence signals was quantified as previously described [40], and the percentage of a fluorescent signal present in punctate structures was quantified as previously described [32]. For 4D videos, quantification of fluorescence signals was performed using custom IMAGEJ plugins [37] as follows. Deconvolved image sequence stacks were bleach corrected for each channel and converted into 4D montage series, which were further converted to 8-bit hyperstacks. For Fig. S1D, all the spots in the average projected time frames except one juxtaposed red and green pair were deleted using the custom plugin described before [37]. IMAGEJ plugin was used to calculate the fluorescence over time for individual punctate structures. Three sets of independent experiments were performed to capture fluorescence microscopy images. In each experiment, 20 images were captured. The total number of images used for analysis were mentioned as 'n' values in the legend. GRAPHPAD PRISM software (GraphPad Software, San Diego, CA, USA) was used to plot all the quantification data in this study. The statistical significance of differences between pairs of samples was determined by a paired two-tailed Student's t-test. P-value < 0.05 was considered statistically significant.

Protein extraction and western blotting

Cells were grown up to log phase (OD at 600 nm–0.5–0.7) in YPD medium and the culture was centrifuged at 1000 g for 3 min. The pellet was washed using SD media and 1XPBS and lysed in Laemmli buffer (50 mM Tris pH 7.4, 2% SDS, 10% glycerol, 1% β-mercaptoethanol, 0.004% Bromophenol blue). The samples were vortexed for a minute and kept in boiling water for 10 min. After boiling they were immediately put on ice for 10 min followed by centrifugation at 15 339 g at RT. Forty microlitre of supernatant was resolved on SDS/PAGE and electro-blotted onto PVDF membranes (Pall Technologies, PALL corporation, New York City, NY, USA). The membranes were blocked in 5% bovine serum albumin (BSA) in Tris-buffered saline containing 0.1% Tween-20 (TBST) for 1 h and then incubated with primary antibody overnight at 4 °C on a rocking platform. Mouse-anti-GFP antibody (Clontech, Takara bio Inc, Kusatsu, Japan, cat no. 632375; dilution1 : 15 000) was used to probe the GFP-fused protein of interest. The next day, the membranes were washed $3\times$ with TBST on an orbital shaker and incubated with secondary antibody (goat-anti-mouse IgG (H + L) secondary antibody, HRP-cat no. - 31430 (Invitrogen, Waltham, MA, USA); dilution – 1 : 5000 in 2.5% BSA in TBST), at room temperature for 1 h on the rocking platform followed by washing $3\times$ with TBST. The proteins were visualized using Advansta Western bright ECL kit (Advansta Inc, San Jose, CA, USA) on Chemidoc MP (Bio-Rad Laboratories, Hercules, CA, USA). Total lane protein visualized by staining the blot with FAST-GREEN served as the loading control.

Results

Characterization of ER–mitochondrial contact structure in *Pichia pastoris*

ER–mitochondria encounter structures (ERMES) were originally identified and well-documented in *S. cerevisiae*. However, *S. cerevisiae* does not have well-defined, distinct ER exit sites, and displays numerous small ER exit sites that collectively form a pattern often misinterpreted as general ER by diffraction-limited fluorescence microscopy. In contrast, *P. pastoris* harbours distinct ER exit sites [26] and ERMES have not been characterized yet in *P. pastoris* making it a better system to examine the relationship between the two sites. Therefore, to check whether ER and mitochondria at all form putative contact sites or regions in *P. pastoris*, we expressed Sec63-mCherry and Tom70-GFP to mark the general ER and mitochondria respectively. Using fluorescent microscopy, we observed that ER and mitochondria tubule indeed overlap/entangle with each other as expected, with some areas of putative close contact between the two organelles (Fig. S1A).

To investigate whether these ER and mitochondria contact structures in *P. pastoris* are genetically conserved to the similar ERMES complex found in *S. cerevisiae*, we fluorescently labelled *P. pastoris* homologs of known subunits of *S. cerevisiae* ERMES (ER–mitochondria encounter structures) with fluorescent proteins. *S. cerevisiae* ERMES complexes are reported to consist of four proteins – Mdm34, Mdm10, Mdm12 and Mmm1 [2,13]. Using sequence homology, we identified

and fluorescently labelled the endogenous *P. pastoris* homologs of Mdm34, Mmm1 and Mdm10 with mGFP and mCherry tags, expecting to label the ERMES complex. As expected, we observed a distinct punctate pattern for both putative ERMES complex homologs, which also co-localized with each other suggesting the discrete presence of ERMES junction in *P. pastoris* (Figs 1A and S1B). To further confirm these results, we also checked the localization of ERMES component Mmm1 with respect to mitochondria (labelled with Tom70-GFP, Fig. 1B) and ER (HDEL-mCherry, Fig. 1C) respectively. As expected, we observed that Mmm1 being the ER component of ERMES localizes on the ER tubule and in proximity to the mitochondria, suggesting the existence of ER–mitochondrial encounter structures (ERMES) in *P. pastoris*. In addition to these, we also observed regions of non-overlapping, but close contact between our target site (ERMES) and the two organelles respectively.

ERMES components lie in juxtaposition to ERES in *Pichia pastoris*

Next, we questioned whether there is any positional correlation between vesicular transport (ERES) and direct membrane contact-mediated mode of inter-organelle communication (ERMES). To investigate, we checked the localization of tagged ERMES proteins with ERES protein Sec13. Interestingly, we observed that ERMES puncta corresponding to components, namely Mmm1 (Fig. 2A), Mdm10 (Fig. 2B) and Mdm34 (Fig. S1C), are juxtaposed with ERES marked with Sec13. The green spots (ERMES) and the red spots (ERES) partially overlap, suggesting spatial proximity between the two sites (Fig. 2C,D). We also observed that not all green spots of ERMES partially overlap with the red spots of ERES; there are some lone ERMES puncta that happen to separate from its corresponding ERES puncta, which suggests that may
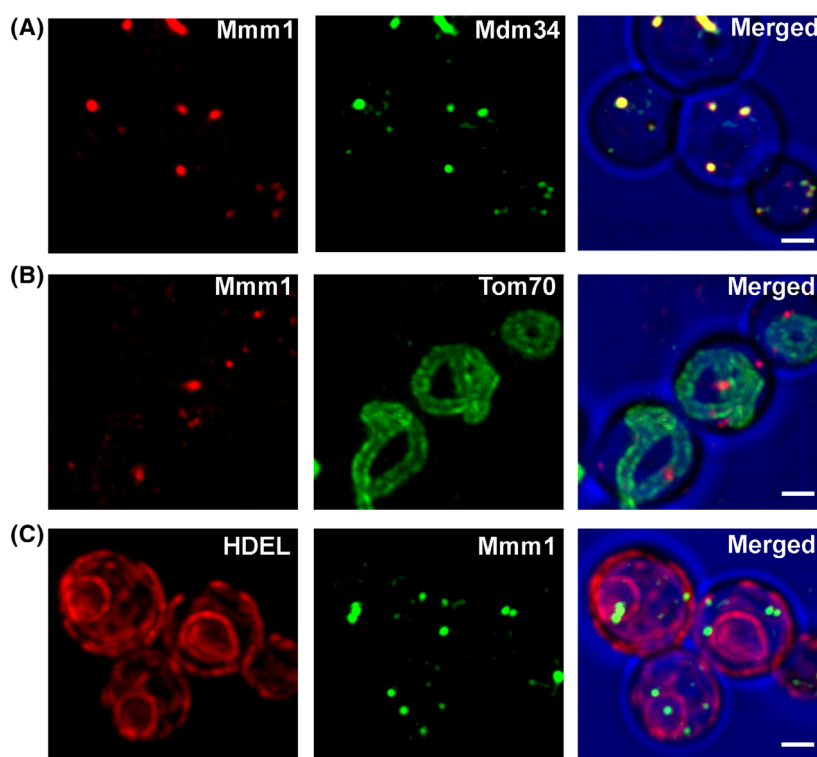

Fig. 1. Characterization of ERMES in *Pichia pastoris*. (A) Localization of ERMES junction complex proteins – Mmm1 and Mdm34 – localize to a punctate pattern, as observed by confocal microscopy. A *Pichia pastoris* PPY12 strain expressing Mmm1-mCherry and Mdm34-GFP. Co-localization of Mmm1, the ER component, and Mdm34, the mitochondrial component, suggest the presence of ERMES junction in *Pichia*. The scale bar represents 1 μm. (B) Relative localization of ERMES component (Mmm1) on mitochondrial tubule marked with Tom70. A strain expressed Mmm1-mcherry and Tom70-GFP. Mmm1 (the ER component) of ERMES junction localized in the vicinity of mitochondria verifying the existence of ERMES in *Pichia pastoris*. The scale bar represents 1 μm. (C) Relative localization of ERMES component (Mmm1) on general ER marked with HDEL. A strain expressed Mmm1-GFP and DsRed-HDEL. Mmm1 (the ER component) of ERMES junction localize on ER tubules verifying the existence of ERMES in *Pichia*. The scale bar represents 1 μm.
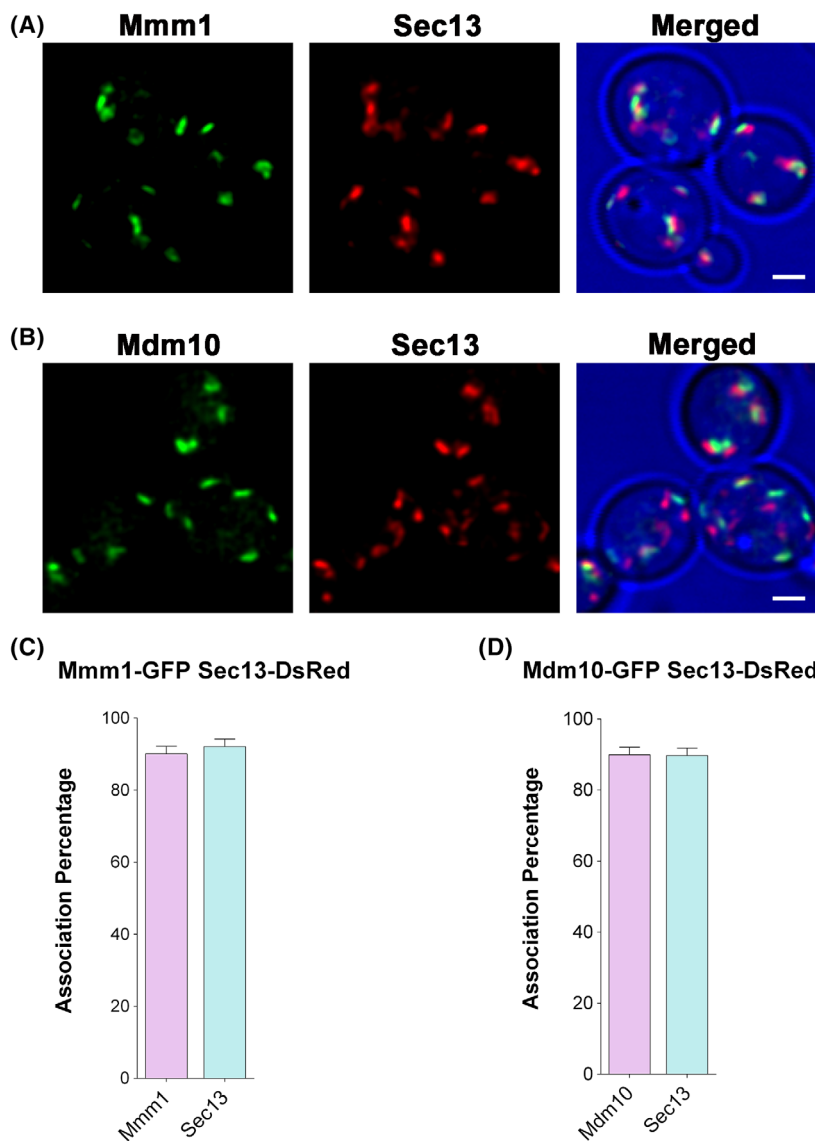
Fig. 2. Relative positioning of ERMES with ERES. (A) Localization of ERMES component Mmm1, with respect to ERES, marked with Sec13. Dual-colour strains expressed Sec13-DsRed with Mmm1-GFP. ERMES component Mmm1-GFP was observed to localize with ERES marked with Sec13 in a juxtaposition manner (localize next to each other) suggesting spatial proximity between the two sites. The scale bar represents 1 μm. (B) Localization of ERMES component Mdm10, with respect to ERES, marked with Sec13. Dual-colour strains expressed Sec13-DsRed with Mdm10 GFP. ERMES component Mdm10 GFP was observed to localize with ERES marked with Sec13 in a juxtaposition manner (localize next to each other) suggesting spatial proximity between the two sites. The scale bar represents 1 μm. (C) Quantification of the data from the (A). Plot showing percentage association between green puncta Mmm1-GFP (ERMES) and its corresponding red puncta Sec13-DsRed (ERES). The number of associated pairs (Mmm1-Sec13) was manually counted for each ~ 60 individual cells. The bar represents SEM. Association percentage count per cell = (No. of associated spots/total no. of green or red spots)*100 ($N = 60$). (D) Quantification of the data from (B). Plot showing percentage association between green puncta Mdm10-GFP (ERMES) and its corresponding red puncta Sec13-DsRed (ERES). The number of associated pairs (Mdm10-Sec13) was manually counted for each ~ 60 individual cells. The bar represents SEM. Association percentage count per cell = (No. of associated spots/total no. of green or red spots)*100 ($N = 60$).

be ERMES and ERES puncta go through cycles of association and disassociation with each other. To further investigate this observation, we measured the percentage association between green puncta (ERMES) and its corresponding red puncta (ERES). Since the green and red spots corresponding to ERMES and ERES instead of totally merging with each other, partially overlap in a sectorial fashion, we manually counted the number of associated green–red spots and the total number of green or red spots per cell to

measure the percentage overlap between ERES and ERMES. We counted 60 cells to plot the data. The following formula was used: Association percentage per Cell = (No. of Associated spots/total no. of green or red spots)*100. We observed approximately 85–90% association between ERMES and ERES, suggesting spatial proximity between the two functional sites of inter-organelle communication (Figs 2C,D and S1D).

ERES forms *de novo* near a pre-existing ERMES most of the time

As we observed that ERMES and ERES associate with each other and share proximity, we were curious to check the dynamic status of ERMES with respect to ERES. Previous studies have reported ERES to be a dynamic structure, and it is formed *de novo* [26]. A recent publication from our lab has shown that the dynamics of ERES with respect to ERAS (ER arrival sites) are indistinguishable, suggesting that these structures are tightly coupled in *P. pastoris* [38]. The key question is whether ERMES is also formed *de novo* and the dynamic nature of the ERMES junction with respect to ERES. For this purpose, we performed 4D imaging following the previously described method [37,38], using ERMES protein Mmm1-GFP and ERES protein Sec13-DsRed as markers (Fig. 3A). As we have previously reported, ERES were observed to form *de novo* and show steady dynamics. ERMES structures were observed to be dynamic, which is not identical to that of ERES dynamics and formation (Fig. 3B). In the 4D movies, we observed the majority of the ERMES puncta remain juxtaposed with ERES from the very beginning (Video S1). We have never seen ERMES forming *de novo*. But we observed that whenever an ERES is forming *de novo*, such formation mostly takes place near a pre-existing ERMES. However, some ERES puncta form independently of the ERMES. To further document the number of times we observed such events (ERES *de novo* formation event juxtaposed to pre-existing ERMES), we manually screened the 4D movies and counted the following type of events – total number of *de novo* ERES formation events occurring per cell, the total number of lone *de novo* ERES formation (not associated with juxtaposed ERMES) and the total number of *de novo* ERES formation event juxtaposed to pre-existing ERMES. Fig. 3C shows the comparative quantification. We found that around 75% of the time, *de novo* formation of ERES happens near a pre-existing ERMES (Fig. 3C). In other words, a pre-existing ERMES usually is found to be near a site where *de*

novo formation of juxtaposed ERES. We also tracked the juxtaposed ERES–ERMES puncta pair in the Mmm1–Sec13 dual-colour strain to document any potential fusion of the ERMES puncta. We observed a plausible fusion of ERMES structures, which is depicted in Fig. S8 (Video S8). However, further detailed studies are needed to document the fusion of ERMES.

Further investigations are necessary to document the physiological significance of the reason why ERES are mostly found to form *de novo* near a pre-existing ERMES. However, the juxtaposition between ERES and ERMES is mostly maintained, suggesting ERMES and ERES are spatially correlated.

Disruption of ERES leads to reduction in ERMES number

ERES and ERMES happen to share spatial proximity. To examine the role of ERES in ERMES formation, we used the anchor-away method to disrupt the ERES and check its effect on ERMES. Previous studies have shown that anchoring away of the COPII inner-layer coat protein Sec23 together with its homolog Shl23, abolished ERES [32]. Therefore, first, to ensure that the ribosomal anchor away of ERES results in mislocalization of the structure (ERES), as a control, we used the strain in which the endogenous Sec23 was tagged by gene replacement with two copies of FRB followed by GFP (FRB2X-GFP/Shl23-FRB). Upon addition of rapamycin, within 5–10 min, a dispersed fluorescence pattern was observed, suggesting that ERES are disrupted (Fig. S2A) [32].

To test the correlation between ERES and ERMES, we checked the localization of Sec23 tagged with FRB2X-GFP Shl23-FRB (same anchor-away strain as explained above) with respect to ERMES protein Mdm34-GFP. In addition to rapamycin, the FRB2X-GFP-tagged Sec23 punctate pattern dispersed (as seen before, Fig. S2A) and concomitantly, the ERMES marker Mdm34 showed a pronounced reduction in puncta number and the spatial overlap between the ERMES (red spots) and the ERES (green spots) was lost (Figs 4A and S2B,C).

To further track the ERES anchor away and its effects on ERMES, we followed the events as a function of time in 4D movies using the same strain as explained above before and after rapamycin treatment. We observed that in control (−rapa), Sec23(ERES) lie in juxtaposition to ERMES(Mdm34) and their spatial proximity is thoroughly maintained during the time course of capture. While in Test (+rapa), Sec23(ERES) puncta got dispersed into the cytosol. Also,
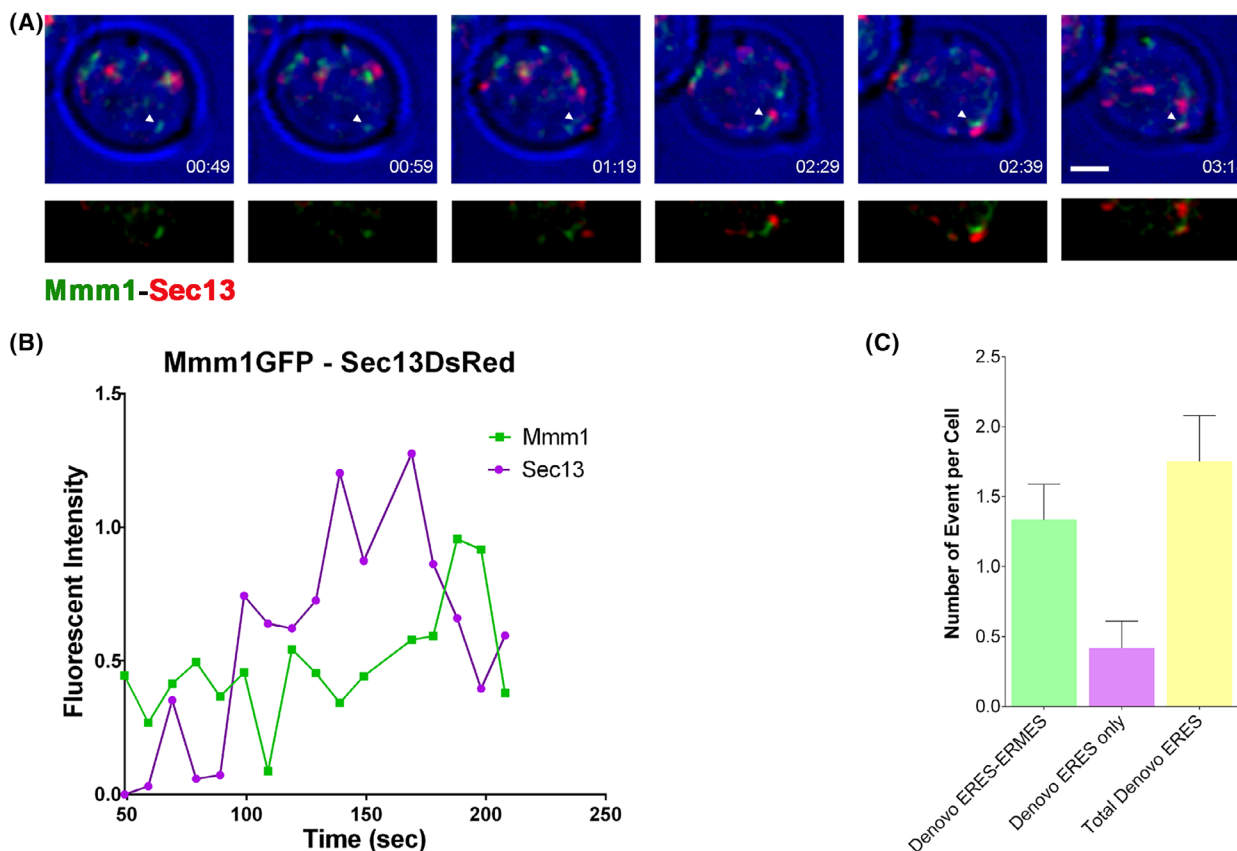
Mmm1-Sec13

Fig. 3. Dynamics of ERMES with respect to ERES. (A) The dynamics of ERMES marked with Mmm1 and ERES marked with Sec13 are not identical, but the juxtaposition of the two sites is mostly maintained. Real-time 4D movies were captured using dual-colour strain-expressing ERES marked with Sec13-DsRed and ERMES marked with Mmm1-GFP on the confocal system. Each 10 min movie was captured and analysed using previously described methods (Materials and methods section). As denoted by arrows, the *de novo* formation of ERES was observed next to a pre-existing ERMES (event). The panel depicted here represents maximum Z projected (stacked) frames from the captured live 4D movie (Video S1). Scale bar, 1 μm. (B) Quantification of the fluorescence signals from the newly formed ERES (red) structures marked by the arrows in (A) that remain associated with pre-formed ERMES (green). The plot shows Mmm1-GFP-labelled spots corresponding to ERMES appear before *de novo* formation of juxtaposed Sec13-DsRed spot corresponding to ERES. However, the spatial proximity between the two areas was maintained throughout. Compared with the Sec13-labelled structures, the Mmm1- labelled structures were more variable and dynamic in shape, so the quantification for Mmm1 was noisier. The *x*-axis of the plot shown here corresponds to the time frames (when the event was observed) from Video S1. (C) Quantification of a number of ERES–*de novo* formation events juxtaposed to pre-existing ERMES. Bar diagram showing the number of *de novo* ERES formations near pre-existing ERMES (represented by the green bar) along with the total number of only *de novo* ERES formations (lone events described by the purple bar) and a total number of ERES *de novo* event (represented by the yellow bar). The captured 4D movies of dual-colour ERMES-ERES strains (expressing Mmm1-GFP marking ERMES and Sec13DsRed marking ERES) were manually screened using IMAGEJ software. This was followed by detecting the ERES *de novo* formation event (new formation of red puncta corresponding to Sec13Ds-Red, across the time frames) and noting the number of times such an event occurred per cell.

pre-existing Sec23 puncta (before rapa addition) appear aggregated and distorted. Concomitantly, the number of Mdm34 puncta is reduced and spatial proximity between the two sites is lost after rapamycin treatment (Fig. S3, Videos S2 and S3). In addition to cytosolic GFP signals, we do see the persistence of some larger GFP spots, possibly representing some kind of aggregation or fusion, a feature we do observe

specifically with this specific strain. Upon anchor away, dispersion of the Sec23 into the cytosol prompted us to ask if the protein was degraded. Western blot confirmed that Sec23 was not degraded (Fig. S6A). Similarly, on anchor away of Sec23-FRB/shl23, GFP-fused Mdm34 also showed no degradation in test and control as confirmed by western blot (Fig. S7B). Nevertheless, 4D movies (Videos S2 and
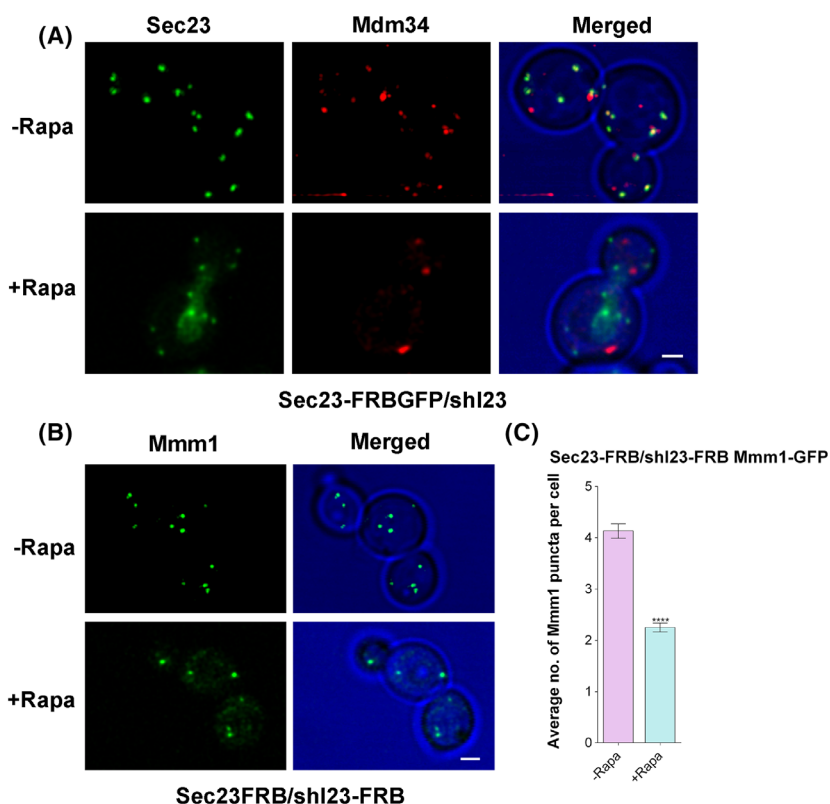
Fig. 4. Effect of disruption of ERES by anchor-away method on ERMES in *Pichia pastoris*. (A) Disruption of ERES by delocalizing COPII components (Sec23-FRB-tagged) leads to a reduction of ERMES (Mdm34) number. A strain expressed Sec23FRBGFP/Shl23-FRB together with the Rpl17-FKBPx4 ribosomal anchor and ERMES marked with Mdm34mCherry. Images were captured before and after treatment with rapamycin (rapa) for 10 min on the confocal system. The addition of rapamycin caused mislocalization of ERES in a spatio-temporal manner showing a dispersed Sec23 punctate pattern while Mdm34 puncta showed a reduction in number in the test (+rapa) versus control (−rapa). The scale bar represents 1 μm. (B) Distribution of ERMES marker Mmm1 before and after the anchor away of ERES component Sec23 and Shl23. A strain expressed Mmm1-GFP together with the Rpl17-FKBPx4 ribosomal anchor as well as Sec23-FRB and Shl23-FRB. Images were captured before and after treatment with rapamycin (rapa) for 10 min on the confocal system. Anchor-away Sec23 (ERES) showed a reduction in the number of Mmm1 puncta in test (+rapa) versus control (−rapa). The scale bar represents 1 μm. (C) Quantification of average number of Mmm1-GFP puncta per cell in test (+rapa) and control (−rapa) sample from (B). A sample of ∼ 60 cells was counted for each of the treated and untreated sets. The plot showed a decrease in the number of Mmm1 puncta (ERMES) in test (treated) versus control (untreated). The bar indicates SEM. **** represents the average number of Mmm1 puncta in the treated sample was significantly lower at $P < 0.0001$.

S3) reveal cytosolic dispersion of the target ERES on getting anchored away.

To further verify this observation, we expressed Mmm1-GFP in a strain-expressing FK506-binding protein (FKBP)-tagged ribosomes as well as Sec23-FKBP-rapamycin-binding domain (Sec23-FRB) and Shl23-FRB [32]. The addition of rapamycin caused the FRB-tagged Sec23/shl23 proteins to be tethered to ribosomes within 5–10 min [32], while the ERMES marker Mmm1GFP showed a pronounced and statistically significant reduction in punctate number (Fig. 4B,C). These results together suggest that the loss of ERES caused a reduction in the number of ERMES junctions.

Disruption of ERMES leads to increased ERES number

To investigate whether the converse, i.e. disruption of ERMES, has any effect on ERES, we decided to delocalize the ERMES subunit Mmm1 (the ER component) by anchor-away technique and check what happens to ERMES junction formation and ERES. As a control, to visualize the effectiveness of ribosomal anchor away of Mmm1, we tagged Mmm1 by gene replacement with FRB-GFP-dual tag. Upon addition of rapamycin, the number of Mmm1 punctate patterns reduced significantly and showed a slight cytosolic dispersion, suggesting that a fraction of Mmm1

(ERMES) has been anchored away successfully (Fig. S4A,B).

Next, we checked the disruption of ERMES (Mmm1-FRBGFP) with respect to another ERMES marker, Mdm34. The addition of rapamycin leads to a statistically significant reduction in the number of Mdm34 puncta, similar to that seen for Mmm1, suggesting that the ERMES junction assembly is affected significantly (Fig. 5A,B). However, in the test, the remaining Mdm34 puncta remained co-localized with the Mmm1 puncta even after 45 min of imaging, suggesting that the ERMES subunits are very tightly bound to one another in the complex. This was further verified by tracking the ERMES anchor away and its effect on the ERMES junction by demonstrating the same in 4D movies, using the same strain as explained above, before and after rapamycin treatment. In 4D movies, the gradual cytosolic dispersion of Mmm1 on anchor away is visualized clearly along with the reduction in ERMES junction (Fig. S5, Videos S4 and S5). The level of Mmm1 is not changed before and after anchoring away as seen by western blotting of the two cell lysates (Fig. S6C).

Next, we checked whether such disruption of ERMES has any implication on ERES. We created an ERMES anchor-away strain by tagging Mmm1 with FKBP-rapamycin-binding domain (FRB) and expressed it in the anchor-away parent strain containing the FKBP (anchored to ribosomes) and ERES marked with Sec31msGFP. Upon the addition of rapamycin, the number of Sec31 puncta (ERES) increased significantly (Figs 5C,D and S5). To confirm whether this was due to increased expression of Sec31, we performed a Western blot to probe GFP-fused Sec31. A marginal increase in the protein expression level was observed in the rapamycin-treated sample than untreated (Fig. S6D,E). Whole-lane protein was used here as the loading control for normalization and quantification of the GFP signal (Fig. S6F).

Furthermore, to check the effects of Mmm1 anchor away on the spatial proximity shared between ERES and ERMES, we created an Mmm1-FRB-GFP strain with ERES labelled by Sec13DsRed. We observed that on the addition of rapamycin, Mmm1-FRB-GFP got mislocalized, resulting in cytosolic dispersion of Mmm1 puncta, which no longer exhibits the typical juxtaposition association with ERES as compared to control (Fig. 5E). The same observation was captured in 4D movies in the same strain before and after rapamycin treatment (Videos S6 and S7).

Additionally, we conducted the following control experiments to rule out non-specific off-target results. The parent anchor-away strain (PPY12/tor1-1/Δfpr1/

RPL-4FKBP-HA [32]) with a different fluorescently labelled reporter is microscopically checked in the presence and absence of rapamycin. The result observed is similar for both rapamycin-treated and untreated strains, which display an unchanged number of Mdm34 (ERMES) puncta or Sec31(ERES) puncta. This strengthened our conclusion that the effect that we observed in the study is indeed due to the effective anchor-away experiment (Fig. S4C,D).

Our results suggest that while partial delocalization of ERMES component prevents the ERMES assembly, such perturbation leads to an increase in ERES number and loss of spatial proximity between ERES and ERMES.

Djp1, an ER-localized chaperone, exhibits a higher association with respect to ERES than ERMES in *Pichia pastoris*

Djp1 is an ER-based chaperone recently implicated in mediating the ER-SURF pathway, a novel transport mechanism of mitochondrial proteins from ER to mitochondria in an ER–mitochondria interface [29]. Djp1 has been proposed to be localized in general ER, and any specificity of localization within the ER was not detected. Moreover, the early route of this ER-SURF pathway is still elusive. As Djp1 has been reported to possess a function involving trafficking between ER and mitochondria, we were intrigued to investigate its localization with respect to ER exit sites and ER–mitochondrial encounter structures.

When we expressed the endogenous Djp1 as GFP fusion in a *P. pastoris* strain labelled with Sec13DsRed, we observed that Djp1 puncta lie adjacent to ERES puncta marked by Sec13, suggesting a very close association between the two (Fig. 6A, upper panel). The association percentage between the red (Sec13) and green (Djp1) spots is measured by manually counting the number of associated green–red spots and the total number of either green/red spots per cell to calculate the percentage overlap between ERES and DJP1 (Fig. 6B). We also checked the association between Djp1 and GFP and mCherry-tagged ERMES protein Mmm1 (Fig. 6A, lower panel) and Mdm34 (Fig. S4A). We observed that Djp1 puncta lie adjacent to ERMES puncta marked by Mmm1, suggesting a close association between the two. Approximately 60–65% association percentage was observed between ERMES and Djp1 (Fig. 6B). We further measured the Pearson coefficient of co-localization between Djp1 with ERES and ERMES. We observed that Djp1 shows more co-localization with ERES compared to ERMES (Fig. S7A).
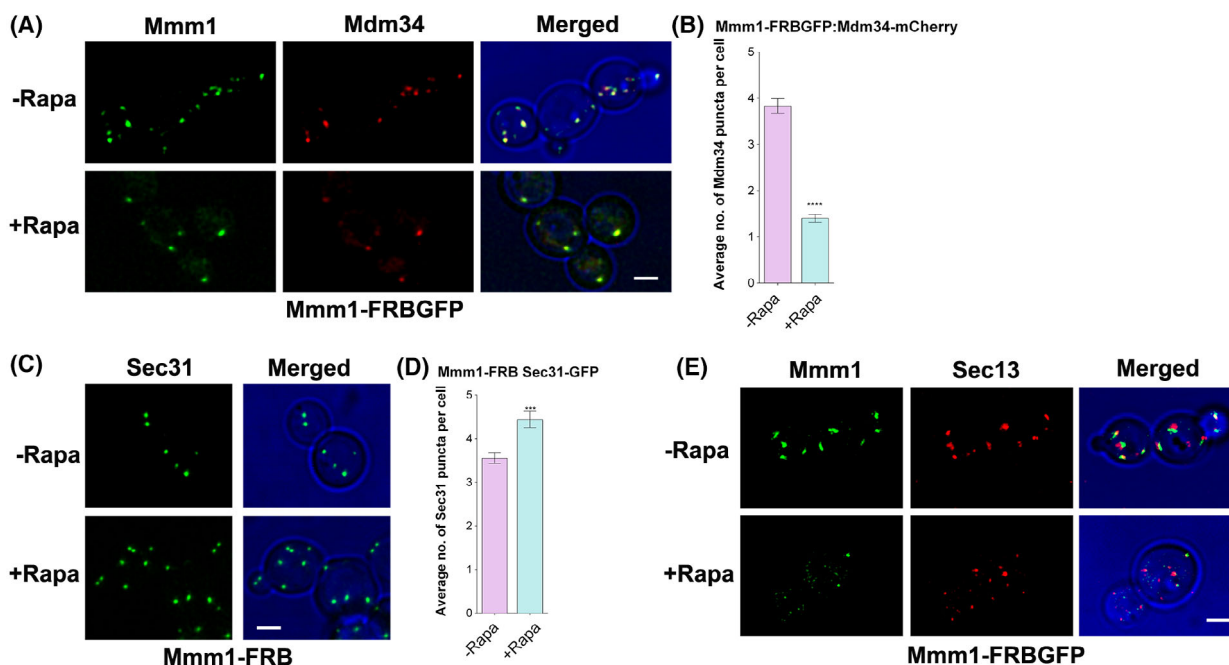
Fig. 5. Effects of disruption of ERMES by anchor-away method on ERMES junction assembly and ERES in *Pichia pastoris*. (A) Redistribution of FRBGFP-tagged Mmm1 (ER component of ERMES) by the anchor-away procedure caused a reduction in the number of ERMES junctions marked with Mdm34mCherry (mitochondrial member of ERMES junction). A strain expressed Mmm1-FRB-GFP together with the Rpl17-FKBPx4 ribosomal anchor and ERMES junction marked with Mdm34mCherry. Images were captured before and after treatment with rapamycin (rapa) for 10 min on the confocal system. Upon addition of rapamycin, Mdm34 puncta show a significant reduction in number in test (+rapa) versus control (−rapa), same as that of Mmm1, suggesting that the number of ERMES junctions formed is affected. The scale bar represents 1 μm. (B) Quantification of average number of Mdm34-GFP puncta per cell in test (+rapa) and control (−rapa) sample. A sample of ∼ 60 cells was counted for each of the treated and untreated sets. The plot showed a decrease in the number of Mdm34 puncta (ERMES) in test (+rapa) versus control (−rapa). The bar indicates SEM. **** represents the average number of Mdm34 puncta in the treated sample was significantly lower at $P < 0.0001$. (C) Effect of ERMES disruption by anchor-away method (Mmm1-FRB) on ERES component (Sec31). A strain expressed Mmm1-FRB together with the Rpl17-FKBPx4 ribosomal anchor and Sec31-msGFP labelling ERES. Images were captured before and after treatment with rapamycin (rapa) for 10 min on confocal system. Upon addition of rapamycin, the number of Sec31 puncta (ERES) showed a slight increment in test (+rapa) as compared to control (−rapa). The scale bar represents 1 μm. (D) Quantification of an average number of Sec31msGFP puncta per cell in rapa treated (+) and untreated (−) samples. A sample of ∼ 60 cells was counted for each of the treated and untreated sets. The plot showed a slight increase in the number of Sec31 puncta (ERES) in test (treated) versus control (untreated). The bar indicates SEM. *** represents the average number of Mmm1 puncta in the treated sample was lower at $P = 0.0001$. (E) Effect of ERMES anchor away (Mmm1-FRBGFP) on ERMES–ERES spatial proximity. A strain expressed Mmm1-FRB-GFP together with the Rpl17-FKBPx4 ribosomal anchor and ERES marked with Sec13-DsRed. Images were captured before and after treatment with rapamycin (rapa) for 10 min on the confocal system. Upon addition of rapamycin, the number of Mmm1 (ERMES) puncta showed a reduction in number, while the number of Sec31 (ERES) showed an increment in test (+rapa) versus control (−rapa), Additionally, the spatial proximity between ERES and ERMES got affected, as the number of associated ERES–ERMES pairs reduced in test (+rapa) as compared to control (−rapa). The scale bar represents 1 μm.

Delocalization of ERES components disrupts Djp1 localization in *Pichia pastoris*

Next, we questioned whether spatio-temporal disruption of ERES has any functional implication on Djp1 localization. We used Sec23 FRB-tagged strain to delocalize COPII, making ERES non-functional [32], and check its effects on the localization of Djp1 tagged with GFP. The addition of rapamycin caused the FRB-tagged proteins (ERES) to get tethered to ribosomes within 5–10 min. We also observed that the Djp1 punctate pattern got completely disrupted in the rapamycin-treated cells compared to control (untreated; Fig. 6C). Our results indicate a specific localization of Djp1 with ERES, which is perturbed when we disrupt ERES assembly. These data suggest that the association of Djp1 with ERES may play a role in its function.

To check whether the delocalization of ERMES constituents has any effect on Djp1, Mmm1 ERMES were disrupted in a spatio-temporal manner using Mmm1-based anchor-away method, and its effects on
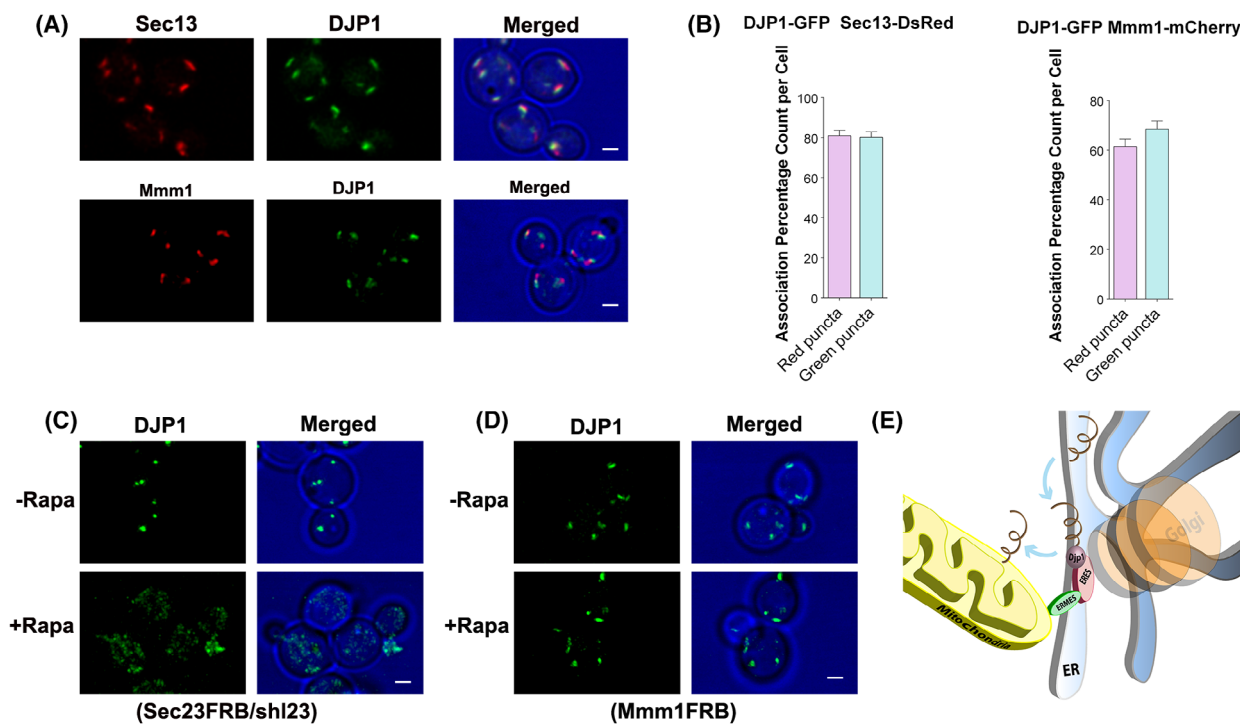
Fig. 6. Localization of Djp1 with respect to ERES, ERMES in *Pichia pastoris* (A) Relative localization of Djp1 with respect to ERES marked by Sec13 (A – upper panel). A strain expressing DJP1-3xGFP and Sec13-DsRed was used. DJP1 puncta localized next to ERES more proximally. (A – lower panel) showed localization of ERMES components, namely Mmm1 with respect to DJP1 respectively. Strains expressing DJP1-3xGFP with Mmm1-mCherry, respectively, were used. DJP1 puncta localized adjacent to ERMES junction marked with Mmm1 with less association. Scale bar represents 1 μm. (B) Quantification of association percentage between DJP1 with ERES (Sec13) and ERMES (Mmm1) respectively (data from A). Djp1 puncta localize in juxtaposition with ERES puncta marked by Sec13 suggesting a very close association between the two (top panel). Plot (left) showing the association percentage between the green (Djp1) spots and the red spots corresponding to Sec13 was measured showing approximately 80% association between ERES and Djp1. However, Djp1 lies adjacent to the ERMES puncta marked by Mmm1 (bottom panel). Plot (right) showing the association percentage between the green (Djp1) spots and the red spots corresponding to Mmm1 was measured showing approximately 60–65% association between ERMES and Djp1. The number of associated pairs, in each of the three cases, was manually counted for each ~ 60 individual cells. The bar represents SEM. Association percentage count per cell = (No. of associated spots/total no. of green or red spots)*100 ($N = 60$). (C) Effects of disruption of ERES by anchor-away method on Djp1 localization. A strain-expressed DJP1-3xGFP together with the Rpl17-FKBPx4 ribosomal anchor as well as Sec23-FRB and Shl23-FRB were used. Images were captured before and after treatment with rapamycin (rapa) for 10 min on the confocal system. Upon addition of rapamycin, the Djp1 puncta got disrupted in test (+rapa) sample as compared to control (−rapa). The scale bar represents 1 μm. (D) Effects of disruption of ERMES component (Mmm1FRB) by anchor-away method on Djp1 localization. A strain-expressed Mmm1-FRB together with the Rpl17-FKBPx4 ribosomal anchor and DJP1-3xGFP. Images were captured before and after treatment with rapamycin (rapa) for 10 min on the confocal system. Upon addition of rapamycin, no significant change in the number of Djp1 puncta was detected in the test sample as compared to control. Scale bar, 1 μm. (E) Model depicting the scheme of how ERES–ERMES spatial proximity aid in the transport of protein from ER to mitochondria *via* Djp1, which gets affected when the juxtapositioning of the two functional sites is abrogated. Localizing at the vicinity of ERES, Djp1 successfully retrieves the mitochondria-bound protein and helps it to go to mitochondria. ERES–ERMES spatial proximity is critical and strongly influences DJP1 localization.

Djp1 were observed using confocal microscopy. Upon the addition of rapamycin, no significant change in the number of Djp1 puncta was detected (Fig. 6D). Thus, loss of ERES dramatically affects Djp1, while disruption of ERMES does not have much effect on Djp1 localization.

Based on these results, we hypothesize that Djp1 must probably be mediating its reported function in mitochondrial protein transport by exploiting ERMES–ERES spatial overlap. Moreover, such a mode of transport possibly is routed through the immediate vicinity of ER exit sites through the association of Djp1 depicted in the model (Fig. 6E).

Discussion

The classical vesicular trafficking pathway has been studied for many years, while direct membrane

contact-based transport is a relatively newer field [32,41–43]. These two communication pathways are well-studied individually, but their potential interplay is unknown. So far, ERMES are primarily documented in *S. cerevisiae*, which lacks distinctive ER exit sites making correlative microscopic documentation of ERES and ERMES challenging. This intrigued us to use *P. pastoris* as a model to check whether there is any correlation between ERES (a well-defined, distinct early secretory component) and ERMES (direct MCS).

We characterized ERMES in *P. pastoris* and observed that ERES and ERMES lie in juxtaposition. Moreover, we found that *de novo* formation of ERES mostly happens near a pre-existing ERMES. Further studies are needed to verify whether ERMES functions as a guide or template for ERES *de novo* synthesis. However, such observations suggest that ERES and ERMES, the two critical sites important for inter-organelle communications, share spatial proximity. The question is whether such physical proximity has functional implications within the cell. We observed that spatio-temporal disruption of either of the two sites, ERES or ERMES, affected the copy number of the other. Previous studies have shown that ERES-associated component such as Sar1GTPase plays a role in influencing the ER–mitochondria contact region [23]. These observations are consistent with the data reported in these studies.

Earlier studies have reported ERMES to play a role in physically bringing ER and mitochondria close to each other so that the exchange of proteins and other biomolecules can occur between the two compartments [2,13,44–46]. Therefore, we hypothesized that such ERES–ERMES proximity might aid mitochondrial protein transport from ER. In support of this theory, a recent study highlighted the involvement of Djp1, an ER-based chaperone, in mediating the transport of cytosol-synthesized proteins like Oxa1 to mitochondria from ER [29] by the ER-SURF pathway. Our study observed that Djp1 showed more spatial association with ERES (80%) than ERMES (60%). Interestingly, upon delocalization of COPII proteins (Sec23/Shl23), Djp1 localization got disrupted. On the other hand, disruption of ERMES does not have much effect on Djp1 localization. Overall, our study highlights that ERES–ERMES physical proximity is possibly critical for ER-SURF pathway-mediated mitochondrial protein import/targeting in *P. pastoris*.

The details of the mechanism by which Djp1 helps transport mitochondrial protein remain unclear. Hansen et al.'s [29] study suggested that Djp1 is localized in the general ER. Our data document that Djp1, a chaperone, localizes at distinct ERES in *P. pastoris*.

So, why was Djp1 previously reported to be at the general ER instead of ER exit sites? ERES localization often can be misinterpreted as a general ER pattern in *S. cerevisiae* as it lacks distinct ER exit sites. Instead, it has numerous tiny ER exit sites that are microscopically challenging to document.

But a question may arise regarding the purpose of Djp1 being localized in ERES? The most plausible answer will argue that the functionality of Djp1 in the ER-SURF pathway demands it to be localized at or in the vicinity of ER exit sites. Djp1 belongs to the DNA-J protein-based family of chaperones. According to the literature, molecular chaperones exist in all cellular compartments where *de novo* protein folding occurs, such as cytosol, ER and mitochondria [47]. Molecular chaperones like the heat shock protein family (Hsp70/Hsp40) and their co-chaperones assist in proper folding, prevent misfolding and aggregation, aid translocation from ER to mitochondria and prepare terminally misfolded proteins for degradation [48]. For Djp1, being localized at ERES possibly make it more efficient to interact with mitochondria-bound cargo directly, retrieve those destined for mitochondria and re-route them via the ER-SURF pathway (Fig. 6E). More generally, the functional role of the Djp1-ERES association is puzzling. We do not have mechanistic insight into such an association at this time, and further studies are needed. ER surface was proposed as an intermediate transit stop for mitochondrial proteins synthesized in the cytosol before traveling to their mitochondria [29]. It may be possible that ERES-bound traffic flow of cargo proteins exists within ER surface along with ER lumen. We can speculate that ER-based chaperones like Djp1 bind and sort out these mitochondria-bound proteins rapidly as soon as they arrive near ERES and target them to mitochondria utilizing ERES–ERMES proximity by an unknown mechanism. Further investigations are needed in the future to document whether ERES–ERMES proximity aids in the mitochondrial protein import function of Djp1. It also remains to be seen whether other potential chaperones specific for various other organelle-bound proteins exist and engage in a similar process for the direct transport of these proteins to their destination organelles.

Acknowledgements

Bhattacharyya lab members for carefully reviewing the manuscript.

Author contributions

Data availability statement

The data that support the findings of this study are available in the main figures and the Supplementary Material of this article.

References

1 Bonifacino JS, Glick BS. The mechanisms of vesicle budding and fusion. *Cell*. 2004;**116**:153–66.

2 Kornmann B, Walter P. ERMES-mediated ER-mitochondria contacts: molecular hubs for the regulation of mitochondrial biology. *J Cell Sci*. 2010;**123**:1389–93.

3 Langhans M, Meckel T, Kress A, Lerich A, Robinson DG. ERES (ER exit sites) and the "secretory unit concept". *J Microsc*. 2012;**247**:48–59.

4 Lang A, John Peter AT, Kornmann B. ER-mitochondria contact sites in yeast: beyond the myths of ERMES. *Curr Opin Cell Biol*. 2015;**35**:7–12.

5 Abrisch RG, Gumbin SC, Wisniewski BT, Lackner LL, Voeltz GK. Fission and fusion machineries converge at ER contact sites to regulate mitochondrial morphology. *J Cell Biol*. 2020;**219**:e201911122.

6 Csordas G, Renken C, Várnai P, Walter L, Weaver D, Buttle KF, et al. Structural and functional features and significance of the physical linkage between ER and mitochondria. *J Cell Biol*. 2006;**174**:915–21.

7 Frank J, Radermacher M, Penczek P, Zhu J, Li Y, Ladjadj M, et al. SPIDER and WEB: processing and visualization of images in 3D electron microscopy and related fields. *J Struct Biol*. 1996;**116**:190–9.

8 Penczek P, Marko M, Buttle K, Frank J. Double-tilt electron tomography. *Ultramicroscopy*. 1995;**60**:393–410.

9 Shore GC, Tata JR. Two fractions of rough endoplasmic reticulum from rat liver. I. Recovery of rapidly sedimenting endoplasmic reticulum in association with mitochondria. *J Cell Biol*. 1977;**72**:714–25.

10 Elbaz-Alon Y, Guo Y, Segev N, Harel M, Quinnell DE, Geiger T, et al. PDZD8 interacts with Protrudin and Rab7 at ER-late endosome membrane contact sites

associated with mitochondria. *Nat Commun*. 2020;**11**:3645.

11 Wu H, Voeltz GK. Reticulon-3 promotes endosome maturation at ER membrane contact sites. *Dev Cell*. 2021;**56**:52–66.e7.

12 Kornmann B. The molecular hug between the ER and the mitochondria. *Curr Opin Cell Biol*. 2013;**25**:443–8.

13 Kornmann B, Currie E, Collins SR, Schuldiner M, Nunnari J, Weissman JS, et al. An ER-mitochondria tethering complex revealed by a synthetic biology screen. *Science*. 2009;**325**:477–81.

14 Kutik S, Stojanovski D, Becker L, Becker T, Meinecke M, Krüger V, et al. Dissecting membrane insertion of mitochondrial beta-barrel proteins. *Cell*. 2008;**132**:1011–24.

15 Meisinger C, Pfannschmidt S, Rissler M, Milenkovic D, Becker T, Stojanovski D, et al. The morphology proteins Mdm12/Mmm1 function in the major beta-barrel assembly pathway of mitochondria. *EMBO J*. 2007;**26**:2229–39.

16 Meisinger C, Rissler M, Chacinska A, Szklarz LKS, Milenkovic D, Kozjak V, et al. The mitochondrial morphology protein Mdm10 functions in assembly of the preprotein translocase of the outer membrane. *Dev Cell*. 2004;**7**:61–71.

17 Takeda H, Tsutsumi A, Nishizawa T, Lindau C, Busto JV, Wenz LS, et al. Mitochondrial sorting and assembly machinery operates by beta-barrel switching. *Nature*. 2021;**590**:163–9.

18 Lee JE, Cathey PI, Wu H, Parker R, Voeltz GK. Endoplasmic reticulum contact sites regulate the dynamics of membraneless organelles. *Science*. 2020;**367**:eaay7108.

19 Krols M, Bultynck G, Janssens S. ER-Mitochondria contact sites: a new regulator of cellular calcium flux comes into play. *J Cell Biol*. 2016;**214**:367–70.

20 Hobbs AE, Srinivasan M, McCaffery JM, Jensen RE. Mmm1p, a mitochondrial outer membrane protein, is connected to mitochondrial DNA (mtDNA) nucleoids and required for mtDNA stability. *J Cell Biol*. 2001;**152**:401–10.

21 Hirabayashi Y, Kwon SK, Paek H, Pernice WM, Paul MA, Lee J, et al. ER-mitochondria tethering by PDZD8 regulates Ca(2+) dynamics in mammalian neurons. *Science*. 2017;**358**:623–30.

22 Hariri H, Bhattacharya N, Johnson K, Noble AJ, Stagg SM. Insights into the mechanisms of membrane curvature and vesicle scission by the small GTPase Sar1 in the early secretory pathway. *J Mol Biol*. 2014;**426**:3811–26.

23 Ackema KB, Prescianotto-Baschong C, Hench J, Wang SC, Chia ZH, Mergentaler H, et al. Sar1, a novel regulator of ER-mitochondrial contact sites. *PLoS ONE*. 2016;**11**:e0154280.

24 Bhave M, Papanikou E, Iyer P, Pandya K, Jain BK, Ganguly A, et al. Golgi enlargement in Arf-depleted

yeast cells is due to altered dynamics of cisternal maturation. *J Cell Sci*. 2014;**127**:250–7.

25 Iyer P, Bhave M, Jain BK, RoyChowdhury S, Bhattacharyya D. Vps74p controls Golgi size in an Arf1-dependent manner. *FEBS Lett*. 2018;**592**:3720–35.

26 Bevis BJ, Hammond AT, Reinke CA, Glick BS. De novo formation of transitional ER sites and Golgi structures in *Pichia pastoris*. *Nat Cell Biol*. 2002;**4**:750–6.

27 Chacinska A, Koehler CM, Milenkovic D, Lithgow T, Pfanner N. Importing mitochondrial proteins: machineries and mechanisms. *Cell*. 2009;**138**:628–44.

28 Neupert W, Herrmann JM. Translocation of proteins into mitochondria. *Annu Rev Biochem*. 2007;**76**:723–49.

29 Hansen KG, Aviram N, Laborenz J, Bibi C, Meyer M, Spang A, et al. An ER surface retrieval pathway safeguards the import of mitochondrial membrane proteins in yeast. *Science*. 2018;**361**:1118–22.

30 Gould SJ, McCollum D, Spong AP, Heyman JA, Subramani S. Development of the yeast *Pichia pastoris* as a model organism for a genetic and molecular analysis of peroxisome assembly. *Yeast*. 1992;**8**:613–28.

31 Sears IB, O'Connor J, Rossanese OW, Glick BS. A versatile set of vectors for constitutive and regulated gene expression in *Pichia pastoris*. *Yeast*. 1998;**14**:783–90.

32 Bharucha N, Liu Y, Papanikou E, McMahon C, Esaki M, Jeffrey PD, et al. Sec16 influences transitional ER sites by regulating rather than organizing COPII. *Mol Biol Cell*. 2013;**24**:3406–19.

33 Goldstein AL, McCusker JH. Three new dominant drug resistance cassettes for gene disruption in *Saccharomyces cerevisiae*. *Yeast*. 1999;**15**:1541–53.

34 Rossanese OW, Soderholm J, Bevis BJ, Sears IB, O'Connor J, Williamson EK, et al. Golgi structure correlates with transitional endoplasmic reticulum organization in *Pichia pastoris* and *Saccharomyces cerevisiae*. *J Cell Biol*. 1999;**145**:69–81.

35 Fitzgerald I, Glick BS. Secretion of a foreign protein from budding yeasts is enhanced by cotranslational translocation and by suppression of vacuolar targeting. *Microb Cell Fact*. 2014;**13**:125.

36 Connerly PL, Esaki M, Montegna EA, Strongin DE, Levi S, Soderholm J, et al. Sec16 is a determinant of transitional ER organization. *Curr Biol*. 2005;**15**:1439–47.

37 Day KJ, Papanikou E, Glick BS. 4D confocal imaging of yeast organelles. *Methods Mol Biol*. 2016;**1496**:1–11.

38 Roy Chowdhury S, Bhattacharjee C, Casler JC, Jain BK, Glick BS, Bhattacharyya D. ER arrival sites associate with ER exit sites to create bidirectional transport portals. *J Cell Biol*. 2020;**219**:e201902114.

39 Schneider CA, Rasband WS, Eliceiri KW. NIH image to ImageJ: 25 years of image analysis. *Nat Methods*. 2012;**9**:671–5.

40 Levi SK, Bhattacharyya D, Strack RL, Austin JR 2nd, Glick BS. The yeast GRASP Grh1 colocalizes with COPII and is dispensable for organizing the secretory pathway. *Traffic*. 2010;**11**:1168–79.

41 Budnik A, Stephens DJ. ER exit sites – localization and control of COPII vesicle formation. *FEBS Lett*. 2009;**583**:3796–803.

42 Miller EA, Barlowe C. Regulation of coat assembly—sorting things out at the ER. *Curr Opin Cell Biol*. 2010;**22**:447–53.

43 Bhattacharyya D, Glick BS. Two mammalian Sec16 homologues have nonredundant functions in endoplasmic reticulum (ER) export and transitional ER organization. *Mol Biol Cell*. 2007;**18**:839–49.

44 Prinz WA. Bridging the gap: membrane contact sites in signaling, metabolism, and organelle dynamics. *J Cell Biol*. 2014;**205**:759–69.

45 Voss C, Lahiri S, Young BP, Loewen CJ, Prinz WA. ER-shaping proteins facilitate lipid exchange between the ER and mitochondria in *S. cerevisiae*. *J Cell Sci*. 2012;**125**:4791–9.

46 Nguyen TT, Lewandowska A, Choi JY, Markgraf DF, Junker M, Bilgin M, et al. Gem1 and ERMES do not directly affect phosphatidylserine transport from ER to mitochondria or mitochondrial inheritance. *Traffic*. 2012;**13**:880–90.

47 Delic M, Valli M, Graf AB, Pfeffer M, Mattanovich D, Gasser B. The secretory pathway: exploring yeast diversity. *FEMS Microbiol Rev*. 2013;**37**:872–914.

48 Kampinga HH, Craig EA. The HSP70 chaperone machinery: J proteins as drivers of functional specificity. *Nat Rev Mol Cell Biol*. 2010;**11**:579–92.

Supporting information

Additional supporting information may be found online in the Supporting Information section at the end of the article.

Table S1. List of Constructs used in the study.

Table S2. List of yeast strains used in the study.

Fig. S1. ER and Mitochondria show putative contact sites in *Pichia pastoris*.

Fig. S2. Effect of anchor away of ERES.

Fig. S3. Effects of functional inactivation of ERES by anchor away technique on ERMES by live-cell tracking.

Fig. S4. Validation of ERMES anchor away strain-in *Pichia pastoris*.

Fig. S5. Effects of functional inactivation of ERMES by anchor away technique on ERMES junction assembly and ERES by live-cell tracking.

Fig. S6. Western Blot to depict the status of protein before and after anchor away of target sites.

Fig. S7. Localization of Djp1 with respect to ERES, ERMES in *Pichia pastoris*.

Fig. S8. Fusion of ERMES with respect to ERES.

Video S1. *De novo* formation of ERES next to a juxtaposed pre-existing ERMES.

Video S2. Effects of ERES anchor away on ERMES. Control (untreated sample) showed no change in the juxtaposed ERES-ERMES pair.

Video S3. Effects of ERES anchor away on ERMES.

Video S4. Effects of ERMES anchor away on ERMES junction assembly.

Video S5. Effects of ERMES anchor away on ERMES junction assembly.

Video S6. Effects of ERMES anchor away on ERES. Control (untreated sample) showed no change in the juxtaposed ERES-ERMES pair.

Video S7. Effects of ERMES anchor away on ERES.

Video S8. Fusion of ERMES next to a juxtaposed ERES.